Measurement of the Reynolds stress tensor using a single rotating slanting hot wire(*)

G. DE GRANDE and CH. HIRSCH (BRUSSEL)

MEASUREMENTS of the six components of the Reynolds stress tensor in a curved duct experiment are reported. The method used is a single rotating slanting hot wire technique. The duct was so constructed that the decay in the outlet section was complete. The most important conclusion from the measurements is that the models describing the turbulent stresses should take into account the history effect of the flow.

Przedstawia się pomiary sześcioelementowego tensora naprężenia Reynoldsa w eksperymencie z zakrzywioną prowadnicą. Zastosowano technikę pojedynczego, obracającego się, nachylonego, gorącego drutu. Prowadnica była tak skonstruowana, że rozpad w rejonie ujścia był kompletny. Najważniejszym wnioskiem otrzymanym z pomiarów było stwierdzenie, że modele opisujące naprężenia turbulentne powinny uwzględniać efekt historii przepływu.

Представлены измерения шестиэлементного тензора напряжений Рейнольдса в эксперименте с искривленной направляющей. Применена техника единичной, вращающейся, наклонной, горячей проволоки. Направляющая была так построена, что распад в районе устья был полным. Самым важным выводом, полученным из измерений, является утверждение, что модели описывающие турбулентные напряжения должны учитывать эффект истории течения.

Nomenclature

A constant in King's law,
A_1, A_2, A_3 constants in the calibration law (4.5),
B constant in King's law,
C_u, C_v, C_w analytical functions in Eq. (4.10),
e fluctuating anemometer output voltage,
E mean anemometer output voltage,
k constant in the calibration law (4.4),
Q mean velocity vector,
u, v, w fluctuating velocity vector components,
U, V, W mean velocity vector components,
U_τ friction velocity,
$\overline{u^2}, \overline{v^2}, \overline{w^2}$ normal turbulent shear stresses,
$\overline{uv}, \overline{vw}, \overline{uw}$ mixed turbulent shear stresses,
x, y, z space coordinates in velocity reference system,
X, Y, Z space coordinates in fixed reference system,
α_0 wire angle,
α_p probe angle, see Fig. 5,
α_{p0} constant angle in Eq. (4.7),
α_R radial or upwash angle, see Fig. 5,

ϕ yaw angle,
ψ "cooling" angle,
τ_w shear stress at the wall.

1. Introduction

IN ORDER to make three-dimensional turbulent boundary layer calculations we are forced to introduce theoretical models in the Navier-Stokes equations for the turbulent stresses. Most of the models used in these calculations are not accurate enough and are almost always based on the mean velocity distributions. As we shall show in our results, this seems to be a very poor supposition and does not include the real behaviour of turbulent stresses in particular and of turbulence in general. Several reasons have led us to the set-up of an experimental program in order to study the behaviour of a three-dimensional turbulent boundary layer. The major reason is the great lack of experimental data on Reynolds stresses in literature. In particular, we wanted to investigate the evolution of a 3-D boundary layer in its growth and, further on, the decay of this boundary layer when transverse pressure gradients disappear.

A study of possible set-ups for the realisation of this experimental program led us to the choise of a curved duct experiment. Measurements of a curved duct experiment are reported in the Ph. D. thesis of VERMEULEN [1]. This work is restricted to the measurement of mean flow values. In the last stations the transverse pressure gradient does not disappear, so we extended the outlet section of our duct in this way that no pressure gradient remained neither in the streamwise nor in the crosswise direction. In a publication by PIERCE and EZEKWE [2] measurements of the Reynolds stresses on the center line of a curved duct are reported but this duct was followed by another circular part so that no comparison would be possible with our data.

In this text measurements made on the upper surface of a curved duct of 60 degrees will be reported. We used a rotating slanting hot wire technique. This technique permits the calculation of the mean flow field and at the same time of the six components of the Reynolds stress tensor. Because only one traverse of the hot wire is needed, the method is very simple and is applicable for every experiment with a minimum of electronic devices.

2. Experimental set-up

A general view of the curved duct is shown in Fig. 1. A two-stage axial compressor of 130 HP supplies the curved duct with air. A convergent of special design is separated from the duct with foam rubber in order to avoid vibration transfer. The 60 degrees curved duct is made of plywood except for the working upper surface made of aluminium plates of 8 mm thick. One hundred and forty holes were drilled in this working surface and sealed with aluminium taps. Pressure tappings bored in these taps served as static pressure holes. Special care was taken to have these taps fit closely in the holes and this neccesitated individual adjusting of the taps. After the duct was set up, the inner surface
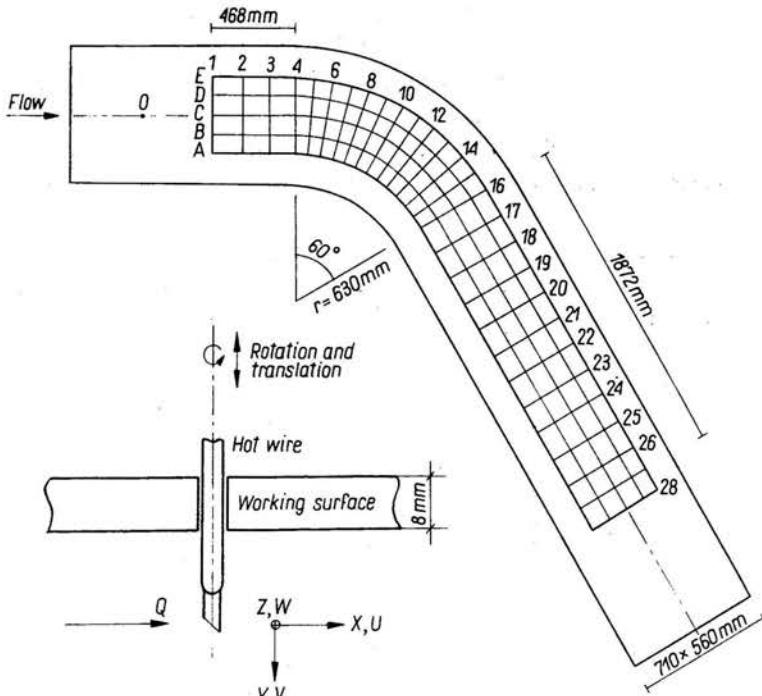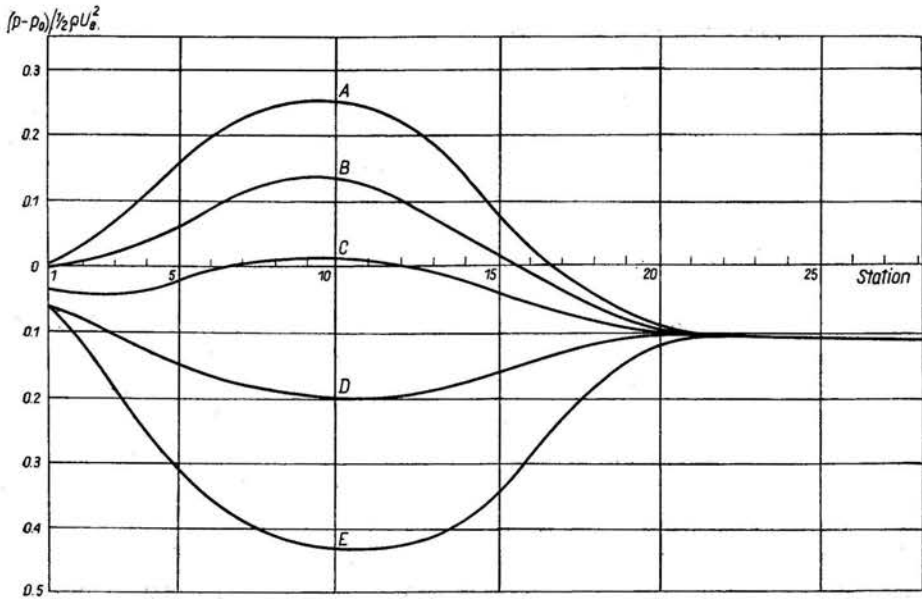
FIG. 1. Curved duct experiment.

FIG. 2. Static pressure distribution over the working surface.

of the working plate was polished to get a smooth surface. Two screens were placed after the convergent for the homogenization of the flow. The probe holder was constructed to permit a vertical and rotating movement of the hot wire. To prevent backlash the measurements were always performed in the same direction. In the early stage of this investigation the resultant velocity profiles were measured with Pitot tubes of different types. These measurements showed that there was no separation on the concave side of the duct.

The static pressure distribution on the working plate can be seen in Fig. 2.

The electronic set-up is shown in Fig. 3. The hot wire anemometer is connected with an integrating digital voltmeter to give the mean anemometer voltage and with an RMS-
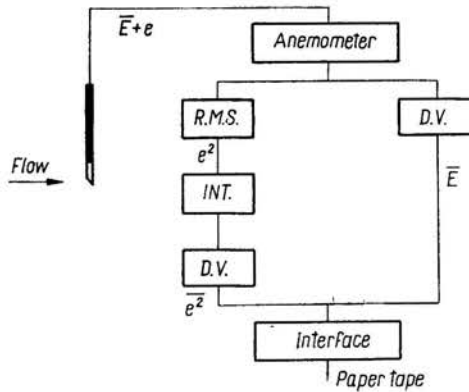

FIG. 3. Electronic set-up.

meter to give the squared fluctuating part e^2 of the anemometer-voltage. An integrator was placed after this RMS-meter so that we could use high time constants for the integration.

The different signals were then punched on paper tape via an interface. This paper tape was read at the computer center and the data were punched on cards. Several programs were then used to calculate the different properties of the boundary layers.

3. Calibration and measuring conditions

The speed of the axial compressor could be adjusted by means of a Ward-Leonard group. The velocity in a reference point 0 at the inlet of the duct was chosen to be 15 m/sec. This velocity was measured with a Pitot tube and the pressure deviations were not higher than 2%. Before and after one measurement, a calibration of the hot wire was performed on a vertical free jet. A directional calibration of the hot wire is not needed because a measurement in one point of the boundary layer can be used as a directional calibration curve. In order to check the repeatability of the measurements, several stations were measured two times and the deviations were in all cases not higher than 3%. Figure 4 presents two velocity reprofiles for the same station, one measurement was made one month after the other.
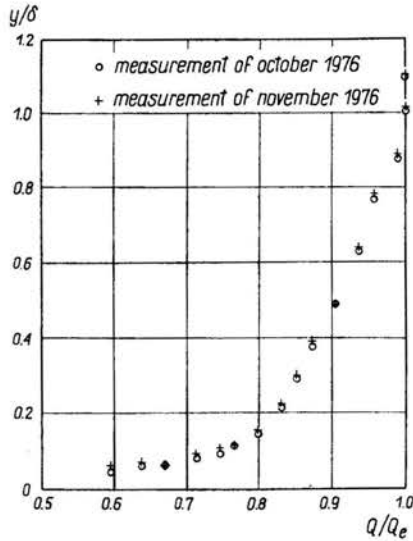
FIG. 4. Resultant velocity measurement.

4. Determination of the Reynolds stress components

In Fig. 5 the configuration of the hot wire put in an air flow is presented. The mean resultant velocity of the flow at the middle of the hot wire is denoted by Q. The X-axis lies in the plane of the hot wire and the prongs. The Y-axis is perpendicular to the wall.
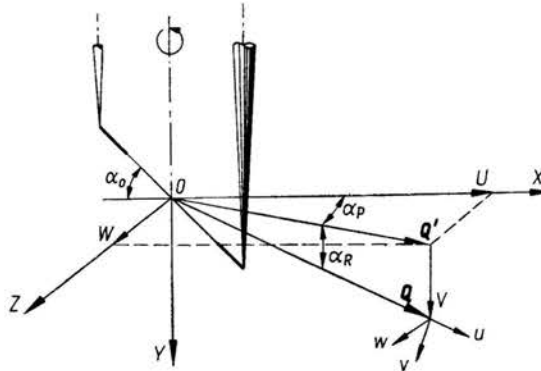

FIG. 5. The geometry of the slanting hot wire.

The radial angle α_R is the angle between the velocity vector Q and its projection on the wall. The angle between the velocity projection on the wall (XZ-plane) and the X-axis is denoted by α_p called probe angle. The hot wire angle is denoted by α_0 and was $45°$ in our experiment. The fluctuating components of the velocity are denoted by u, v, and w. u has.

the same direction as Q, w lies in a plane parallel to the XZ plane and v is perpendicular to the uw plane. With this geometry it is quite easy to prove the following relationship:

(4.1) $$\sin\phi = \cos\alpha_R\cos\alpha_p\cos\alpha_0 + \sin\alpha_0\sin\alpha_R$$

with ϕ = yaw angle.

In most cases the radial angle α_R is supposed to be 0, but it should be mentioned that this is not a restriction of this method.

The cooling of the hot wire is caused by the so-called cooling velocity or effective velocity V_e. This effective velocity is proportional to the magnitude of the velocity and is a function of the angle ϕ between the velocity vector and the hot wire. The calibrations of the hot wire are performed in the following conditions:

$$\alpha_R = 0° \quad \text{and} \quad \alpha_p = \pm 90° \quad \text{with varying velocity.}$$

Plotting the anemometer voltage against the effective velocity V_e results in a relation, called King's law, we have

(4.2) $$E^2 = A + BV_e^n.$$

The constants A, B and n can be calculated using an optimization program. In Eq. (4.2) the effective velocity is expressed as

(4.3) $$V_e = Qf(\phi).$$

The function f describes the directional sensitivity of the hot wire and can be found by rotating the hot wire around its axis. A commonly used expression for this function is

(4.4) $$f^2(\phi) = \cos^2(\phi) + k^2\sin^2(\phi),$$

where k is dependent on the diameter to the length ratio of the hot wire. In our experiment we wanted to take into account the asymmetrical behaviour of the hot wire response. This behaviour is caused by, for example, the unequal dust distribution on the hot wire, resulting in different maxima of the anemometer voltage for the positions $+90°$ and $-90°$ of α_p.

Starting from Eq. (4.1), we may introduce an angle ψ responsible for the cooling of the hot wire and defined as

(4.5) $$\sin\psi = A_1\left(\cos\frac{\alpha_p}{A_2}\cos\alpha_0\cos\alpha_R + \sin\alpha_0\sin\alpha_R\right),$$

where A_2 is a correction factor for the position of the maxima.

Now we may write a simple cosine law for the directional sensitivity of the hot wire:

(4.6) $$V_e = Q\cos\psi.$$

Taking into account the different cooling velocities for different angles of α_p, we then have

(4.7) $$E^2 = A + BV_e^n\left|1 + \frac{\alpha_p}{\alpha_{p_0}}(1 - \text{sign}(1, \alpha_p))A_3\right|^n,$$

where

$$\alpha_{p_0} = \pm A_2\cos^{-1}(\text{tg}\,\alpha_0\,\text{tg}\,\alpha_R).$$

The constant A_3 can be calculated from the position of the maxima in the directional calibration curves. Remark that for positive angles of α_p this correction term becomes zero.

Whatever the expression of the directional response looks like, the following analysis is in general applicable:

$$(4.8) \qquad E = g(V_e(Q, \alpha_0, \alpha_p, \alpha_R)).$$

A finite increase of the anemometer voltage can then be written as

$$(4.9) \qquad e = dE = \frac{dg}{dV_e}\left(\frac{\partial V_e}{\partial Q}dQ + \frac{\partial V_e}{\partial \alpha_0}d\alpha_0 + \frac{\partial V_e^{\cdot}}{\partial \alpha_p}d\alpha_p + \frac{\partial V_e}{\partial \alpha_R}d\alpha_R\right).$$

As the hot wire angle is a constant: $d\alpha_0 = 0$.

The differences dQ, $d\alpha_p$ and $d\alpha_R$ are then related to the fluctuating velocity components. Equations (4.9) then yields

$$(4.10) \qquad e = \frac{dg}{dV_e}(C_u u + C_w w + C_v v).$$

The coefficients are analytical functions of the angles α_0, α_p and α_R, depending on the form of the directional calibration relations. Squaring and averaging of Eq. (4.10) then yields

$$(4.11) \qquad \frac{\overline{e^2}}{\left(\frac{dg}{dV_e}\right)^2} = A_{uu}\overline{u^2} + A_{ww}\overline{w^2} + A_{vv}\overline{v^2} + A_{uv}\overline{uv} + A_{uw}\overline{uw} + A_{vw}\overline{vw}.$$

The calculation of the 6 components of the Reynolds stress tensor is theoretically possible if we measure 6 different values of $\overline{e^2}$ for different angular positions of the hot wire. In practice we need more measurements. In our experiment the value of $\overline{e^2}$ was measured in a range of 200° for the probe angle α_p. Using an optimization program the 6 components of the Reynolds stress tensor could be determined. Some authors like BISSONETTE [3] and So and MELLOR [4] state that a calculation method as explained in the foregoing is doubtful but their measurements were performed using a rotating mechanism which reduces the integration time of the RMS values. Indeed when the hot wire is rotated by means of a continuously driving motor unit, the integration time should be smaller than the angular rotation time. The only inconvenience of the method is a rather large time needed for the registration of the measurements.

5. Experimental results

5.1. Mean velocity field

As already mentioned before, the method enables us to calculate the mean velocity profiles. These mean data are then compared with existing theoretical profiles used in integral calculation methods. The consistency of the mean data values can then be checked by making up the momentum balance using the integral momentum equations. As an
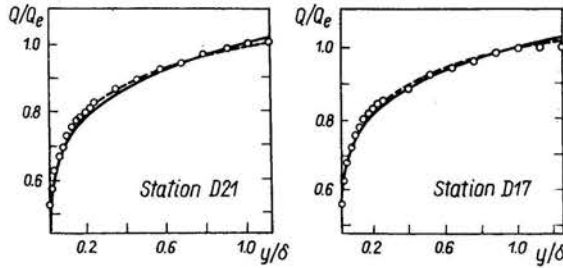
FIG. 6. Resultant velocity profile fitted with a power law (———) and with Coles' law (– – –).

example, we have plotted the velocity profiles in stations D 17 and D 21. In Fig. 6 one can see the resultant velocity profiles compared with the power law and with Coles' law. Figure 7 shows a comparison of the crossflow velocity profile with a Mager and an Eichelbrenner model. A logarithmic plot of the resultant velocity profile with the Coles' law is shown in Fig. 8. This fit was used for the determination of the shear stress at the wall.
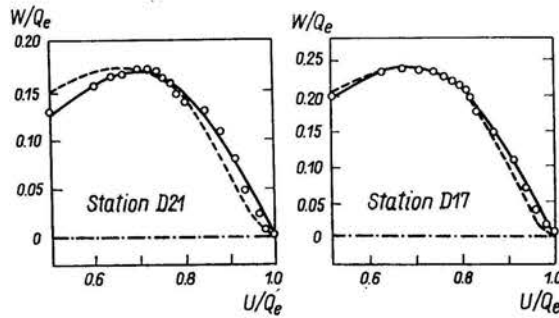
FIG. 7. Cross-flow velocity vs. mean flow velocity fitted with Eichelbrenner (———) and Mager (– – –) laws.
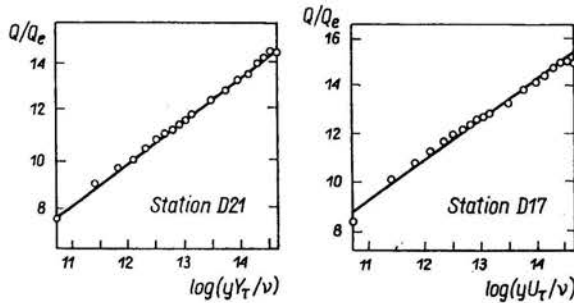

FIG. 8. Clauser plot of resultant velocity profile.

5.2. Reynolds stresses

In this section we shall only discuss the turbulent structure on the A line. Line A lies at the suction side of the duct, so the pressure gradient is negative in the first part and

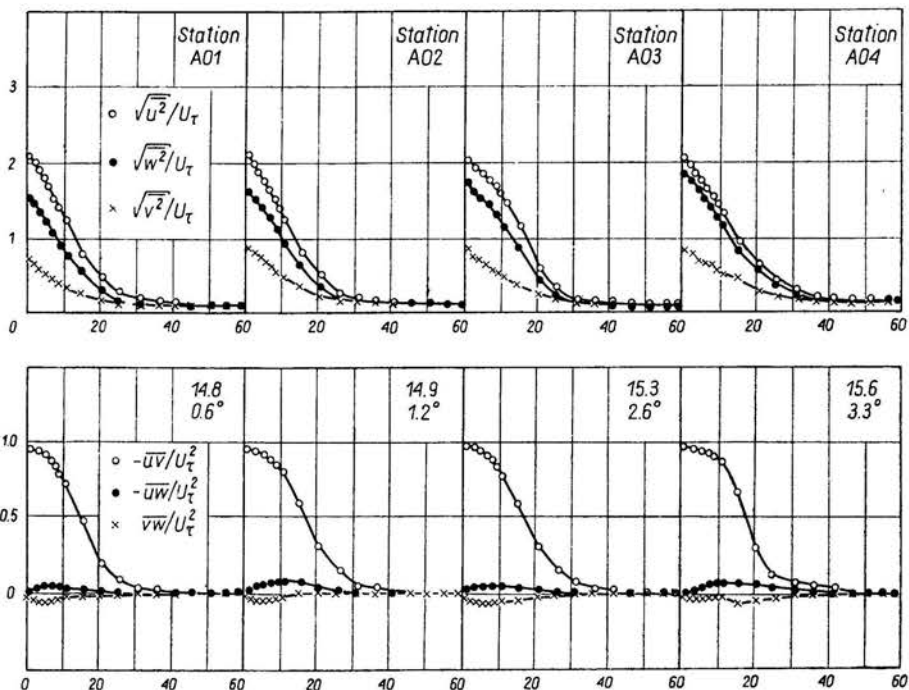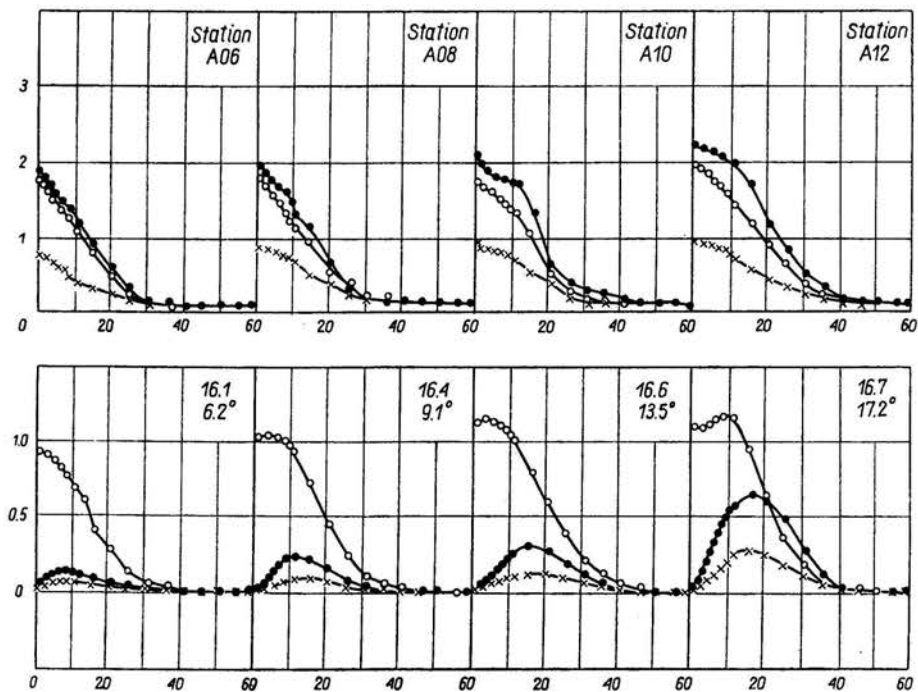FIG. 9a. Reynolds stress tensor along the *A* line.
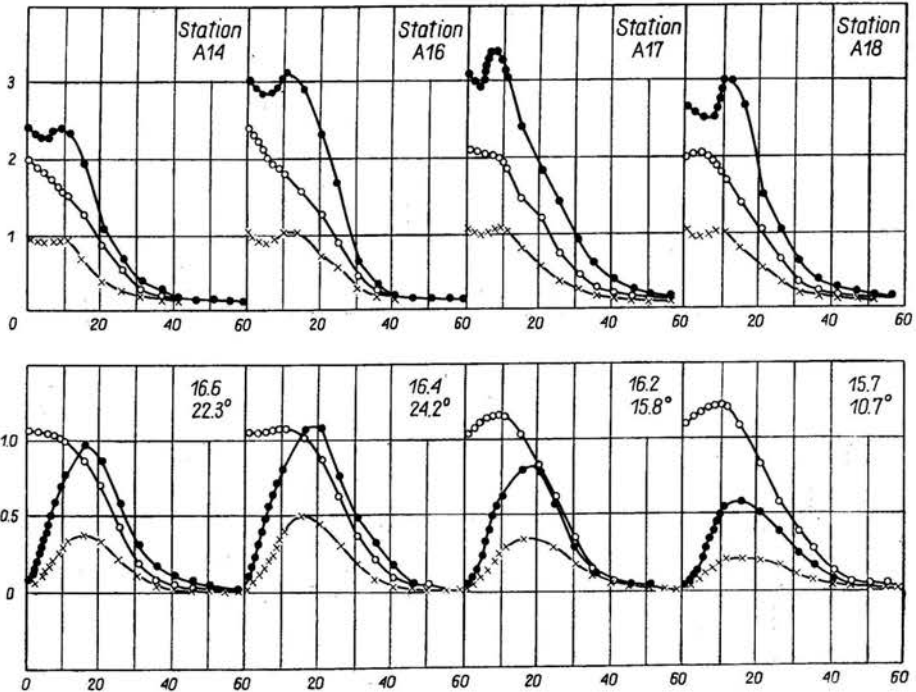

FIG. 9b. Reynolds stress tensor along the *A* line.

[29]

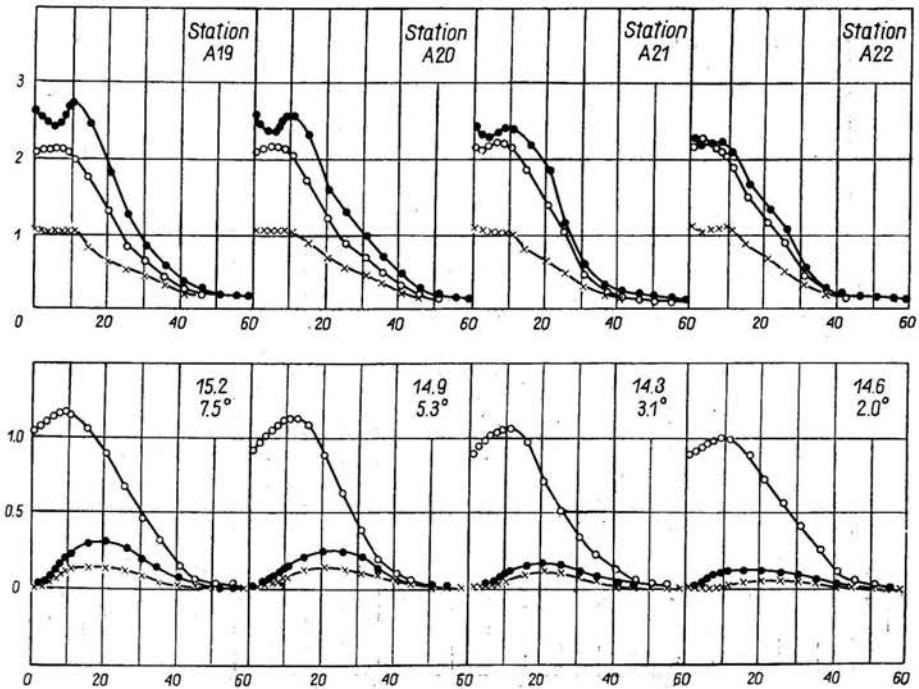FIG. 9c. Reynolds stress tensor along the *A* line.

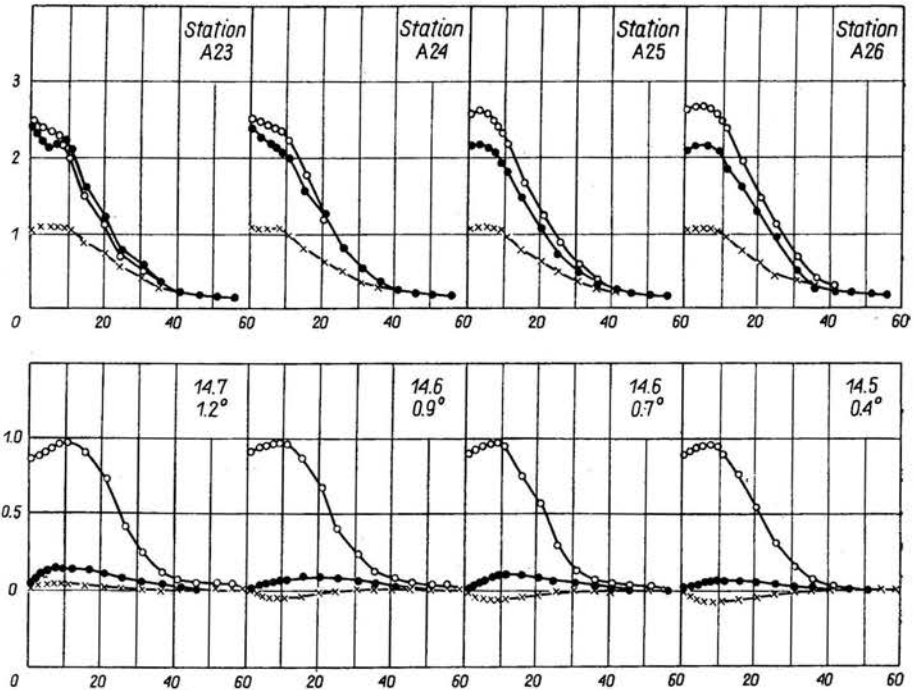FIG. 9d. Reynolds stress tensor along the *A* line.

FIG. 9e. Reynolds stress tensor along the A line.

positive in the second. The velocity in the external flow is decreasing in the first part up to station 12. The production of the normal stress $\overline{u^2}$ is written as

$$-\overline{u^2}\,\frac{\partial U}{\partial x},$$

so the production of this component is decreasing and this can be seen in Figs. 9. It is seen too that the production of $\overline{w^2}$ is increasing; the term describing the production of this stress can be written as

$$-\overline{w^2}\,\frac{\partial W}{\partial z}.$$

As the crossflow is more pronounced at the pressure side of the duct and as the gradient is always positive, the production should be increasing on all lines. Compared with the KLEBANOFF [5] results on a flat plate in a two-dimensional boundary layer, the relative magnitude of the normal stresses is preserved; however, the $\overline{v^2}$ component is somewhat smaller. This is due to the different development of the boundary layers. The boundary layer in the first stations was about 20 mm thick. As can be seen in the figure of the skewing angles at the wall, there is an upstream propagation of the three-dimensional pressure field in the curved duct. This can also be seen at the presence of the $\overline{uw}$ and $\overline{vw}$ components. As the wall shear stress equals τ_w/ϱ at the wall, the shear stress $\overline{uv}/U_\tau^2$ should tend to 1 at the wall ($\overline{vw}$ and $\overline{uw}$ become zero at the wall). This tendency can be seen in Figs. 9. A decrease of the $\overline{u^2}$ component and an increase of the $\overline{w^2}$ stress can be

seen from station 1 to 10. From station 12 the $\overline{u^2}$ stress is increasing up to the last station but this increase is more pronounced from station 12 to station 20. This corresponds to the rise in static pressure along the second part of the line A. There is an increase in $\overline{w^2}$ from station 1 to station 17. Station 17 does not correspond to the maximum in the skewing angles at the wall. However, in this station the maximum amplitude in W is reached.

There is an increase of the $\overline{uw}$ and $\overline{vw}$ components up to station 16 where the $\overline{uw}$ stress becomes larger than the Reynolds stress $\overline{uv}$. However, the contribution to the total production of the turbulent energy is governed by this $\overline{uv}$ stress because the derivatives of U with respect to y is the largest.

6. Conclusion

We have described a method for the measurement of the six components of the Reynolds stress tensor. This survey is very limited and the obtained results are in extenso discussed in the thesis [6]. This thesis includes the calculation of the production and dissipation of the turbulence and it is hoped that this contribution will give further information in the understanding of the difficult field of turbulence.

References

1. A. J. Vermeulen, *Measurements of three-dimensional turbulent boundary layers*, Ph. D. Thesis, Univ. Cambridge, 1971.
2. F. J. Pierce, S. H. Ezekwe Jr., *Measurements of the Reynolds stress tensor in a three-dimensional turbulent boundary layer*, Technical Report, Virginia 1974.
3. L. R. Bissonnette, *An experimental study of the development of a three-dimensional turbulent boundary layer under rapidly changing rate of strain*, Ph. D. Thesis, Princeton Univ., 1970.
4. R. M. C. So, G. L. Mellor, *An experimental investigation of the turbulent boundary layer along curved surfaces*, NASA Report CR-1940, Princeton Univ., 1972.
5. P. S. Klebanoff, *Characteristics of turbulence in a boundary layer with zero pressure gradient*, NACA Technical Notes, 3178, 1954.
6. G. M. J. de Grande, *Three-dimensional incompressible turbulent boundary layers*, Ph. D. Thesis, Vrije Univ. Brussel, 1977.

DEPARTMENT OF FLUID MECHANICS
VRIJE UNIVERSITET OF BRUSSEL, BELGIUM.